Understanding SARS-CoV-2 budding through molecular dynamics simulations of M and E protein complexes

Logan Thrasher Collins[1,2,*], Tamer Elkholy[1,3], Shafat Mubin[1,4], Ricky Williams[1,5], Kayode Ezike[1,6], Ankush Singhal[1,7]

[*]Corresponding author; [1]Conduit Computing; [2]Washington University in St. Louis, Department of Biomedical Engineering; [3]Zapata Computing; [4]Valdosta State University, Department of Physics; [5]Harvard University, Department of Electrical Engineering; [6]Attune; [7]Leiden University, Department of Chemistry

Abstract:
SARS-CoV-2 and other coronaviruses pose a major threat to global health, yet treatment efforts have largely ignored the process of envelope assembly, a key part of the coronaviral life cycle. When expressed together, the M and E proteins are sufficient to facilitate coronavirus envelope assembly. Envelope assembly leads to budding of coronavirus particles into the ER-Golgi intermediate compartment (ERGIC) and subsequent maturation of the virus, yet the mechanisms behind the budding process remain poorly understood. Better understanding of budding may enable new types of antiviral therapies. To this end, we ran atomistic molecular dynamics (MD) simulations of SARS-CoV-2 envelope assembly using the Feig laboratory's refined structural models of the M protein dimer and E protein pentamer. Our MD simulations consisted of M protein dimers and E protein pentamers in patches of virtual ERGIC membrane. By examining how these proteins induce membrane curvature *in silico*, we have obtained insights around how the budding process may occur. In our simulations, M protein dimers acted cooperatively to induce membrane curvature. By contrast, E protein pentamers kept the membrane planar. These results could help guide the development of novel antiviral therapeutics which inhibit coronavirus budding.

Introduction:

The global COVID-19 pandemic has highlighted the need for diverse ways of responding to infectious disease. Though vaccines, diagnostics, and treatments have all helped combat SARS-CoV-2, the pandemic continues to wreak havoc across our world. Furthermore, the looming threat of coronavirus variants which might counter vaccine efficacy remains concerning. While much has been learned about the biology of SARS-CoV-2, some aspects of its life cycle still represent areas of mystery. It is of paramount importance to develop new tools for fighting coronaviruses, so gaining improved understanding of understudied parts of the SARS-CoV-2 life cycle may open valuable doors.

In order to form infectious particles, coronaviruses must undergo a process known as envelope assembly.[1] This process facilitates budding of nucleocapsid-containing particles into the ERGIC. When expressed together without the help of any other coronavirus proteins, the M and E proteins are sufficient to allow budding of virus-like particles (VLPs) which resemble those produced by wild-type coronaviruses.[2–4] The exact mechanisms by which the M and E proteins contribute to budding remain unclear. Some have proposed that coronavirus M proteins oligomerize into a matrix layer to induce membrane curvature,[5,6] though more recent data on SARS-CoV-2 has indicated that its M proteins do not form a matrix layer.[7] The role of the E protein in budding is also poorly understood, though it is thought to interact with the M protein in some way and perhaps coordinate envelope assembly.[6,8,9] It should be noted that the M protein is roughly 300 times more abundant in the ERGIC than the E protein.[10] Expression of the

nucleocapsid N protein has also been shown to greatly enhance the yield of budding VLPs compared to when only the M and E protein are present.[11] By contrast, the famous S protein is not strictly required for coronavirus budding, though it is incorporated into the VLPs when expressed alongside M and E.[3] Because of their vital role in budding, the M and E proteins represent key components of the coronavirus life cycle.

Therapeutics targeting SARS-CoV-2 have largely ignored the budding process. This is unfortunate since the E and M proteins tend to be highly conserved across many coronavirus species.[12] Drugs which target budding might therefore act as pan-coronaviral treatments. So far, computational drug repurposing efforts have identified a variety of existing medicines with potential bioactivity against the SARS-CoV-2 papain-like protease, main 3C-like protease, and RNA-dependent RNA polymerase (RdRp), helicase, 3'-to-5' exonuclease, 2'-O-ribose methyltransferase, endoRNase, and spike-ACE2 interface.[13] Using these computational approaches as a foundation, the most successful drug repurposing treatments have involved compounds targeting the RdRp, the proteases, and the spike-ACE2 interface.[14] Monoclonal antibody therapeutics have focused on the spike protein as a result of its exposure on the surface of SARS-CoV-2 particles.[15,16] Though some interest has been shown in blocking the E protein's ability to act as an ion channel,[17,18] it is unclear as to whether this would interfere with budding itself or with some other aspect of SARS-CoV-2 physiology.[9] To date, there are no therapeutics which disrupt coronavirus budding.

Molecular dynamics (MD) simulations can help to better understand biological phenomena, yet there has not been much work involving MD and coronavirus budding. Monje-Galvan and Voth recently performed MD simulations which characterized the movements of single M protein dimers and E protein pentamers in virtual ERGIC membrane.[19] This revealed various insights around individual M dimers and E pentamers, including that the M protein dimer can introduce local deformations in the membrane. However, their study did not investigate how multiple interacting M dimers and E pentamers might influence membrane curvature, which is important for understanding SARS-CoV-2 budding. Yu et al. reported a coarse-grained MD investigation of the completed SARS-CoV-2 virion, which included numerous M, E, and S proteins.[20] Though the study did involve all of the three structural proteins, it focused on the completed spherical virus, so the roles of the structural proteins in budding were not examined. There remains a need for MD simulations of the budding process which interrogate how multiple SARS-CoV-2 structural protein complexes may work to facilitate budding.

We utilize atomistic molecular dynamics simulations to investigate the roles of the M and E protein complexes in budding. Because of the lack of complete crystal structures of the M and E proteins, we use the Feig laboratory's predicted structural models of the M protein dimer and E protein pentamer.[21] We construct membrane patches with lipid composition mimicking that of the mammalian ERGIC and insert M protein dimers and E protein pentamers into the virtual membranes. Our investigation uses six systems: a membrane-only system (mem), a system with a single E protein pentamer in membrane (1E), a system with four E protein pentamers in membrane (4E), a system with a single M protein dimer in membrane (1M), a system with four M protein dimers in membrane (4M), and a system with three M protein dimers and one E protein pentamer in membrane (3M1E). We observe that the 4M system exhibits strong cylindrical curvature, with M protein dimers working cooperatively. By contrast, the rest of the systems show minimal curvature, including the 3M1E system. We observe that E protein pentamers keep the membrane relatively planar. Our results suggest that blocking the actions of the M protein dimers might serve

as a viable route for antiviral therapeutics that target budding. We hope that our results may guide the first steps towards the development of therapeutics which disrupt the budding process.

Results:

Atomistic simulations of the six systems (mem, 1E, 1M, 4E, 4M, and 3M1E) were performed using GROMACS and visualized using VMD. All six systems were solvated using explicit water molecules and ions. Mem was run for 887 ns, 1E was run for 1256 ns, 4E was run for 971 ns, 1M was run for 1102 ns, 4M was for 955 ns, and 3M1E was run for 468 ns. From our observations in VMD, we noted that that the 4M system gained a substantial degree of curvature over the course of the simulation (Fig. 1A), while other systems such as mem had much less curvature (Fig. 1B). We characterized protein dynamics by using the software MDanalysis[22] to perform root-mean-square deviation (RMSD) (Fig. 2A-E) and radius of gyration (R_g) (Fig. 3A-E) calculations for all of the proteins across the five systems which contained proteins. To characterize membrane curvature, we first split our trajectories into 100 ns subintervals (0-100 ns, 300-400 ns etc.) and used the g_lomepro software package[23] to compute 2D time-averaged curvature heatmaps (Fig. 4A-F) and 3D time-averaged curvature plots (Fig. 5A-F) for selected subintervals over the six systems. These analyses allowed us to interrogate the mechanisms of SARS-CoV-2 budding.

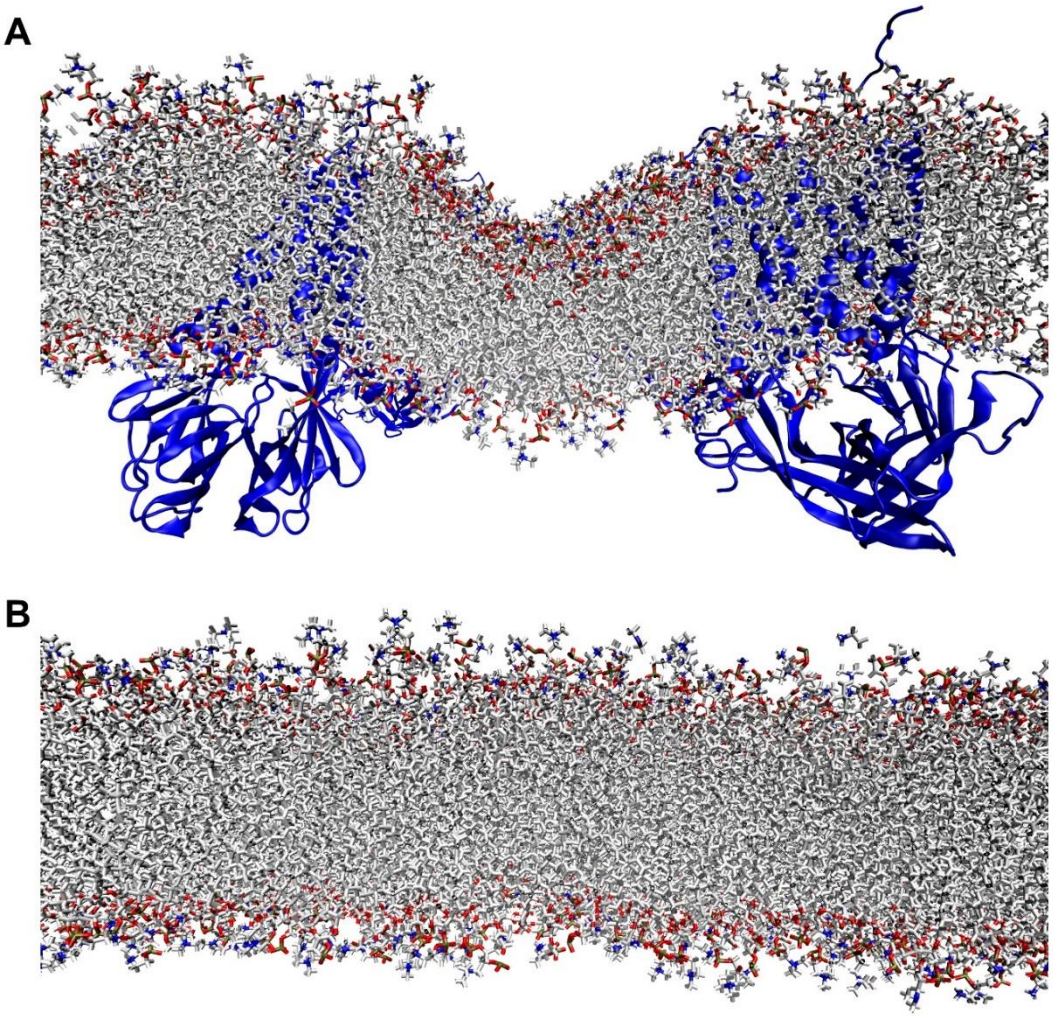

Figure 1 Representative side-view snapshots of **(A)** the high level of curvature in the 4M system at 800 ns and **(B)** the lack of curvature in the mem system at 800 ns.

RMSD calculations revealed some key differences between the M and E proteins. The E proteins consistently reached higher RMSD compared to the M proteins (Fig. 2A-E). This is likely due to the flexible hinge regions connecting the cytosolic α-helices to the transmembrane α-helices. When we visualized the E proteins in VMD, we observed that their cytosolic α-helices tended to undergo free rotations about their flexible hinge regions, leading to a wide array of configurations (Fig. 3A). When we visualized the M proteins in VMD, we did not qualitatively observe as much flexibility in their cytosolic domains (Fig. 3B). The lack of flexibility in the M proteins may facilitate retention of their wedgelike shape, which could help induce membrane curvature. We tentatively suggest that the less restricted motion of the E protein cytosolic α-helices could play a role in sequestering M proteins to coordinate budding. As such, the differences in flexibility between the M protein and E protein cytosolic domains may provide hints as to their functional mechanisms and possible ways of disrupting those mechanisms.

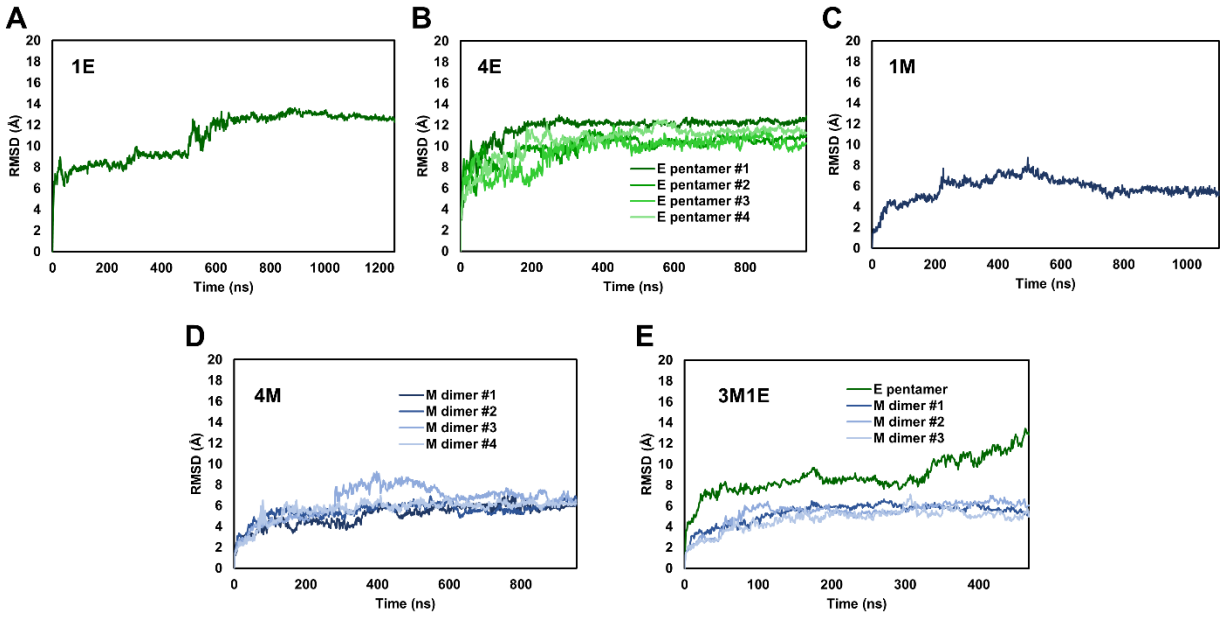

Figure 2 RMSD over time for **(A)** the 1E simulation, **(B)** the 4E simulation, **(C)** the 1M simulation, **(D)** the 4M simulation, and **(E)** the 3M1E simulation.

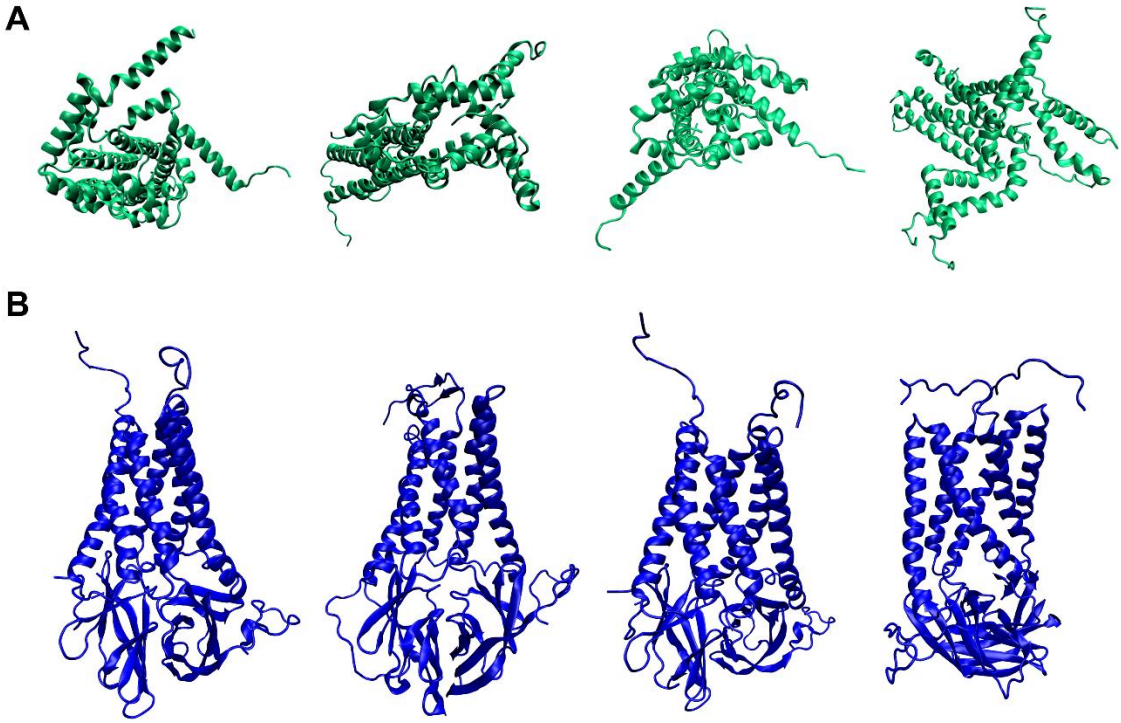

Figure 3 Representative snapshots of protein configurations. **(A)** The configurations of each of the E protein pentamers in the 4E system at 900 ns. For clarity, the E proteins are shown with their cytosolic domains pointing towards the viewer. **(B)** The configurations of each of the M protein dimers in the 4M system at 900 ns. For clarity, the M proteins are shown from the side.

R_g calculations supported similar conclusions about the M proteins and E proteins (Fig. 4A-E). The R_g values of the M proteins remained relatively constant over their time courses. For all of the M protein dimers across the 1M, 4M, and 3M1E systems, the R_g values were roughly the same. The R_g values of the E proteins tended to decrease slightly over their time courses. Between individual E protein pentamers across the 1E, 4E, and 3M1E systems there was greater variability among the R_g plots. These data support the notion that the M protein dimers have relatively rigid conformations while the E protein pentamers may have looser structures. The reason that the E proteins might exhibit such loose structures is likely due to the previously mentioned flexible hinges between their transmembrane and cytosolic domains. As mentioned, the relative rigidity of the M proteins may help them retain their wedgelike shape when inducing membrane curvature. These R_g data corroborate the results of the RMSD data and offer clues as to how the M and E proteins may function in SARS-CoV-2 budding.

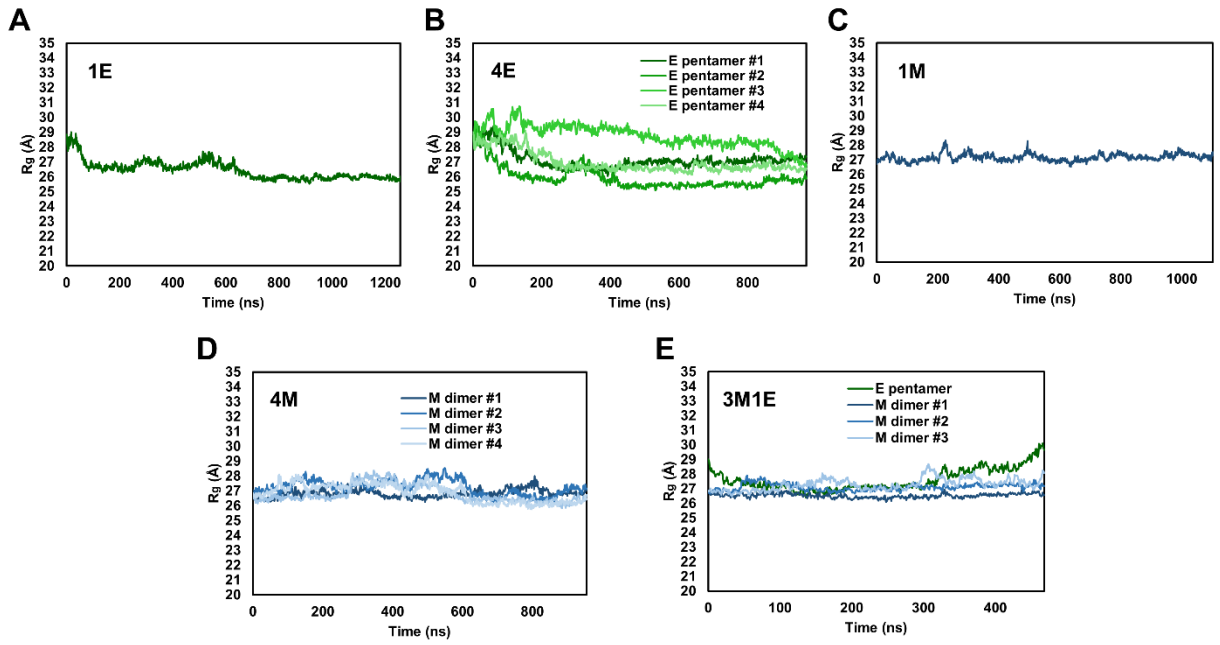

Figure 4 R_g over time for **(A)** the 1E simulation, **(B)** the 4E simulation, **(C)** the 1M simulation, **(D)** the 4M simulation, and **(E)** the 3M1E simulation.

We employed the g_lomepro software[23] to generate 2D time-averaged mean curvature heatmaps of all six systems (Fig. 5A-F) as well as 3D plots of the same data (Fig. 6A-F). For the 1E system, we generated mean curvature averaged over 0-100 ns and over 1100-1200 ns (Fig. 5A, Fig. 6A). Only small amounts of curvature are visible in any of the 1E heatmaps or 3D plots. For the 4E system, we generated mean curvature averaged over 0-100 ns and over 800-900 ns (Fig. 5B, Fig. 6B). Only small amounts of curvature are visible in any of the 4E heatmaps or 3D plots. For the 1M system, we generated mean curvature averaged over 0-100 ns and over 900-1000 ns (Fig. 5C, Fig. 6C). In the upper leaflet of the membrane, the 1M system shows a small region of curvature corresponding to the single M protein dimer. The region of curvature appears in the 0-100 ns time period but is more pronounced over the 900-1000 ns time period. Even alone, M protein dimers may exhibit geometric properties which can induce kinks in the membrane. For the 4M system, we generated mean curvature averaged over 0-100 ns and over 800-900 ns (Fig. 5D, Fig. 6D). In the 0-100 ns period, only a small amount of curvature is present. Over the 800-900 ns period, strong curvature can be seen. The curvature profile seen in the 4M system heatmaps and 3D plots likely corresponds to the curve of the membrane seen in snapshots of the 4M system. For the 3M1E system, we generated mean curvature averaged over 0-100 ns and over 300-400 ns (Fig. 5E, Fig. 6E). Several scattered bulges are visible in both the 0-100 ns and 300-400 ns periods, probably corresponding to the M protein dimers. However, the kind of cooperative activity seen in the 4M system does not appear to occur in the 3M1E system, possibly due to the shorter timescale of the simulation. For the mem system, we generated mean curvature averaged over 0-100 ns and over 700-800 ns (Fig. 5F, Fig. 6F). Very little curvature is visible in any of the mem heatmaps or 3D plots. These data indicate that E proteins likely do not induce substantial curvature, that isolated M proteins create small bulges in the membrane, and that many M proteins together can act cooperatively to induce larger amounts of curvature.

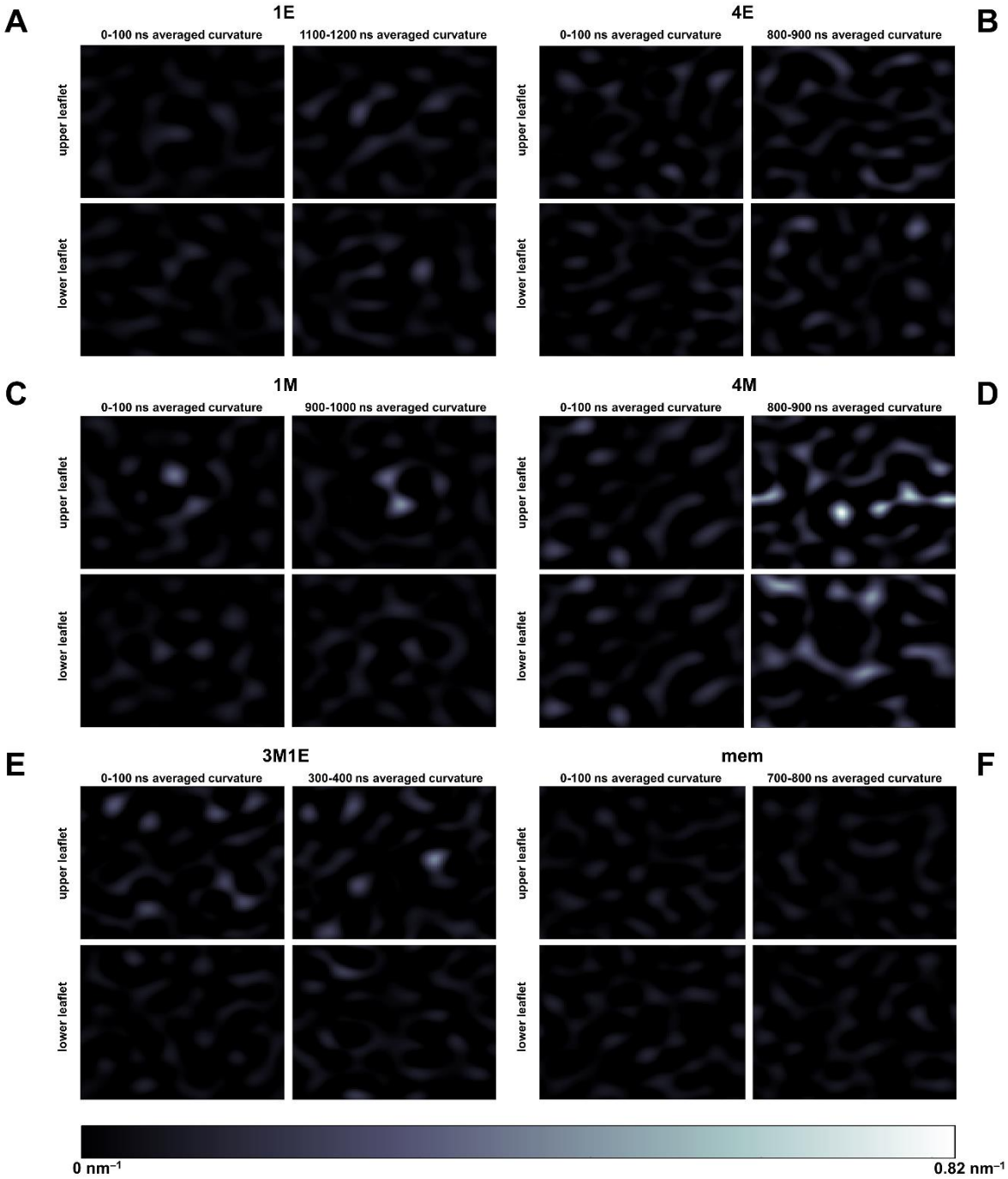

Figure 5 Mean curvature heatmaps of the upper and lower membrane leaflets as averaged over the indicated 100 ns time periods for **(A)** the 1E simulation, **(B)** the 4E simulation, **(C)** the 1M simulation, **(D)** the 4M simulation, **(E)** the 3M1E simulation, and **(F)** the mem simulation.

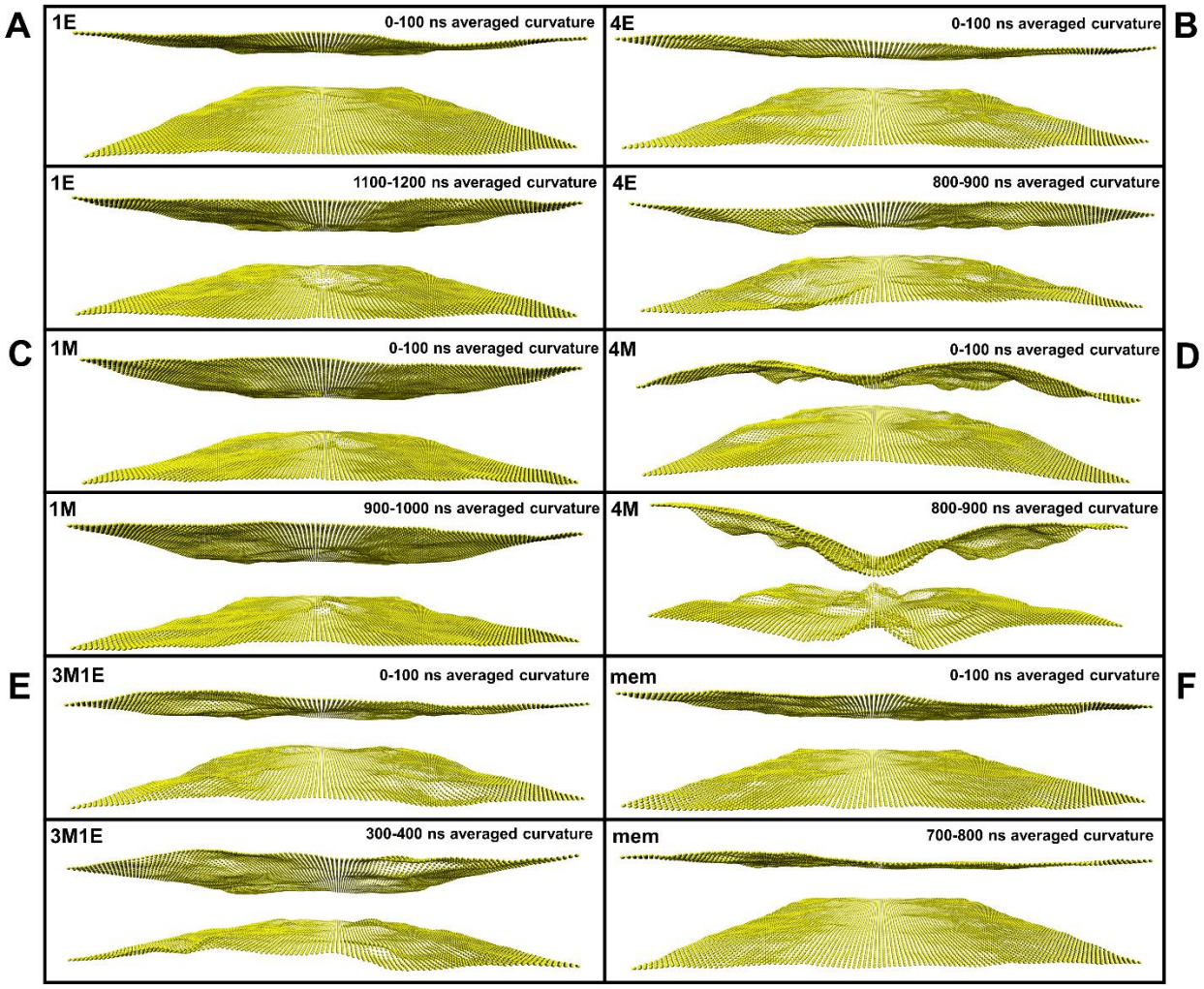

Figure 5 Mean curvature 3D plots as averaged over the indicated 100 ns time periods for **(A)** the 1E simulation, **(B)** the 4E simulation, **(C)** the 1M simulation, **(D)** the 4M simulation, **(E)** the 3M1E simulation, and **(F)** the mem simulation.

Discussion:

Our atomistic MD simulations revealed insights around the likely roles of M and E proteins in the budding of SARS-CoV-2. In our simulations, multiple M proteins induced membrane curvature in a cooperative fashion. E proteins did not induce substantial membrane curvature and even appeared to interfere with the cooperative actions of M proteins in the 3M1E system. Furthermore, the M protein dimers showed consistently lower RMSD values and less variable R_g values than the E protein pentamers, indicating that the M proteins had more overall rigidity. These insights may help steer the design of therapeutics which could interfere with coronavirus budding.

Through our RMSD and R_g calculations, we found lower levels of flexibility in the M protein dimer structures as compared to the E protein pentamers. This may have arisen from the unstructured hinge regions linking the cytosolic and transmembrane α-helices of the E proteins. By comparison, the cytosolic domains of the M protein dimer structures were large globular structures consisting mostly of β-sheets, so steric hindrance may have kept those domains from

moving as freely as the cytosolic α-helices of the E proteins. We suggest that the wedgelike shape of M protein dimers coupled with their stiffness may help them to sculpt the host membrane towards curvature. This is evident from the small bulges introduced by M protein dimers in the 1M and 3M1E systems and from the strong overall curvature seen with the cooperative actions in the 4M system. Differences between M proteins and E proteins may facilitate distinct functions.

We showed *in silico* how SARS-CoV-2 may induce membrane curvature at an atomistic scale. In our 1M and 3M1E simulations, small bulges appeared around the regions where M protein dimers were located. This suggests that even individual M protein dimers possess the necessary geometry to introduce kinks into the host membrane. In our 4M simulation, the four M protein dimers worked together to induce strong curvature in the membrane. Because coronaviruses are known to produce large numbers of M proteins in the ERGIC membranes of infected cells,[10] we hypothesize that this cooperative effect might increase further in the biological reality, leading to enough curvature to encapsulate the RNA genome and associated nucleocapsid of the virus. The lack of consistent curvature in the 1E, 4E, and 3M1E simulations indicates that the E protein likely does not directly facilitate membrane curvature during SARS-CoV-2 budding. However, since experimental results indicate that E proteins are essential for budding coronaviruses,[2–4] the E protein still probably plays another important role in budding. One possibility is that the E protein introduces a planar region into the membrane's overall curvature, eventually creating a viral envelope with a larger radius of curvature than would be possible with only the M proteins. That said, the actions of the E proteins might occur over longer scales of space and time than were possible in our models. Our simulations suggest that M proteins are responsible for the membrane curvature observed in coronavirus budding.

Based on the results of our simulations, we propose that the M protein dimer may represent a valuable target for drugs intended to treat COVID-19 and other coronavirus diseases. Due to the high level of conservation of the M protein across different types of coronaviruses,[12] we postulate that a drug affecting the M protein might have a broad degree of efficacy. Some possible mechanisms for such drugs include disruption of the wedgelike geometry of the M dimer, complete destabilization of the interface between the two M protein monomers, or blockage of the cooperative activity among multiple M protein dimers. The latter might involve designing drugs which interfere with interactions between the cytosolic domains of distinct M dimers. Pharmaceuticals which target the M protein could provide a powerful approach by which to mitigate the effects of coronaviral infections.

Methods:

Six MD simulations of M and E proteins in lipid membrane were used in this study. All of the simulations were carried out at atomic resolution using GROMACS 2019.4.[24] Structures of the E protein pentamer and M protein dimer were obtained from the Feig laboratory's predicted models.[21] Six initial configurations were constructed: a membrane-only system (mem), a system with a single E protein pentamer in membrane (1E), a system with four E protein pentamers in membrane (4E), a system with a single M protein dimer in membrane (1M), a system with four M protein dimers in membrane (4M), and a system with three M protein dimers and one E protein pentamer in membrane (3M1E). To mimic the biological ERGIC, the membrane composition used for all six systems was as follows: 57% POPC, 25% POPE, 10% POPI, 2% POPS, 6% Cholesterol.[21] All the systems were solvated using explicit water molecules and ions. The CHARMM36 force field[25] was used for all lipids, ions, and proteins, while the TIP3P[26] model was implemented for the water molecules. All hydrogen atoms were constrained with the LINCS

algorithm,[27] and long-range electrostatics were evaluated with particle-mesh Ewald summation.[28] All simulations used 2 fs time step with Leap-Frog integrator[29] and a 1.4 nm cutoff for all of the interactions. A standard energy minimization procedure was performed using the steepest descent method.[30] For each simulation, a small NPT equilibration run was performed followed by a production run using a Nose-Hoover thermostat[31] at 300K and a Parrinello-Rahman barostat[32] at 1 atm. The lengths of the production runs were as follows: 887 ns for mem, 1256 ns for 1E, 971 ns for 4E, 1102 ns for 1M, 955 ns for 4M, and 468 ns for 3M1E. These computational approaches facilitated completion of the simulations.

Analyses of the results of the simulations included RMSD, R_g, and time-averaged mean curvature of the membranes. MDanalysis[22] was used to calculate RMSD and R_g while g_lomepro[23] was used for the membrane curvature calculations. Each protein's RMSD was calculated at 0.1 ns intervals by comparing its conformation at a given time step to a reference conformation consisting of the initial equilibrated structure. To correct for the effects of proteins undergoing translations and rotations during the simulation runs, RMSD was adjusted by translating with a vector $\mathbf{t}$ and rotating with a matrix $\mathbf{R}$. In this way, only the changes in the proteins relative to their initial reference structures were included in the final RMSD outputs. The RMSD was calculated using the coordinates of all of the α-carbon atoms in the given protein where $\mathbf{x}$ describes the coordinates in the current conformation, $\mathbf{x}_{\mathrm{ref}}$ are the coordinates of the reference conformation, and n is the number of α-carbon atoms in the protein.

$$\mathrm{RMSD} = \frac{1}{n}\sum_{i=1}^{n} |(\mathbf{R}\cdot\mathbf{x}_i + \mathbf{t}) - \mathbf{x}_{\mathrm{ref}}|$$

Similarly, R_g was calculated for the α-carbon atoms of each protein at 0.1 ns intervals to analyze changes in the compactness of the proteins. R_g was computed using the displacement vector $\mathbf{r}$ between a given protein's center of mass and each α-carbon of that protein. These calculations were weighted by the mass m of the atom in question.

$$\mathrm{R_g} = \sqrt{\frac{\sum_{i=1}^{n} m_i|\mathbf{r}_i|^2}{\sum m_i}}$$

For membrane curvature calculations, the g_lomepro[23] software package was used to calculate mean curvature as averaged over the frames of the 0-100 ns time periods for all six simulations. This software was also used to calculate mean curvature for selected later time periods in each simulation. These included 1100-1200 ns for 1E, 800-900 ns for 4E, 900-1000 ns for 1M, 800-900 ns for 4M, 300-400 ns for 3M1E, and 700-800 ns for mem. Performing quantitative analyses helped us to decipher insights from our simulations.

Acknowledgements:
Time and resources on the Frontera supercomputer were awarded to Conduit through the COVID-19 High-Performance Computing Consortium project MCB200139.

Conflict of interest:
The authors are affiliated with Conduit Computing, a company which is developing a home diagnostic test for COVID-19 (as well as other infectious diseases) called nanoSPLASH.

References:

(1) Masters, P. S. The Molecular Biology of Coronaviruses; Academic Press, 2006; Vol. 66, pp 193–292. https://doi.org/10.1016/S0065-3527(06)66005-3.

(2) Mortola, E.; Roy, P. Efficient Assembly and Release of SARS Coronavirus-like Particles by a Heterologous Expression System. *FEBS Lett.* **2004**, *576* (1), 174–178. https://doi.org/https://doi.org/10.1016/j.febslet.2004.09.009.

(3) Vennema, H.; Godeke, G. J.; Rossen, J. W.; Voorhout, W. F.; Horzinek, M. C.; Opstelten, D. J.; Rottier, P. J. Nucleocapsid-Independent Assembly of Coronavirus-like Particles by Co-Expression of Viral Envelope Protein Genes. *EMBO J.* **1996**, *15* (8), 2020–2028. https://doi.org/10.1002/j.1460-2075.1996.tb00553.x.

(4) Baudoux, P.; Carrat, C.; Besnardeau, L.; Charley, B.; Laude, H. Coronavirus Pseudoparticles Formed with Recombinant M and E Proteins Induce Alpha Interferon Synthesis by Leukocytes. *J. Virol.* **1998**, *72* (11), 8636 LP – 8643. https://doi.org/10.1128/JVI.72.11.8636-8643.1998.

(5) Neuman, B. W.; Kiss, G.; Kunding, A. H.; Bhella, D.; Baksh, M. F.; Connelly, S.; Droese, B.; Klaus, J. P.; Makino, S.; Sawicki, S. G.; Siddell, S. G.; Stamou, D. G.; Wilson, I. A.; Kuhn, P.; Buchmeier, M. J. A Structural Analysis of M Protein in Coronavirus Assembly and Morphology. *J. Struct. Biol.* **2011**, *174* (1), 11–22. https://doi.org/https://doi.org/10.1016/j.jsb.2010.11.021.

(6) Siu, Y. L.; Teoh, K. T.; Lo, J.; Chan, C. M.; Kien, F.; Escriou, N.; Tsao, S. W.; Nicholls, J. M.; Altmeyer, R.; Peiris, J. S. M.; Bruzzone, R.; Nal, B. The M, E, and N Structural Proteins of the Severe Acute Respiratory Syndrome Coronavirus Are Required for Efficient Assembly, Trafficking, and Release of Virus-Like Particles. *J. Virol.* **2008**, *82* (22), 11318 LP – 11330. https://doi.org/10.1128/JVI.01052-08.

(7) Klein, S.; Cortese, M.; Winter, S. L.; Wachsmuth-Melm, M.; Neufeldt, C. J.; Cerikan, B.; Stanifer, M. L.; Boulant, S.; Bartenschlager, R.; Chlanda, P. SARS-CoV-2 Structure and Replication Characterized by in Situ Cryo-Electron Tomography. *Nat. Commun.* **2020**, *11* (1), 5885. https://doi.org/10.1038/s41467-020-19619-7.

(8) Duart, G.; García-Murria, M. J.; Grau, B.; Acosta-Cáceres, J. M.; Martínez-Gil, L.; Mingarro, I. SARS-CoV-2 Envelope Protein Topology in Eukaryotic Membranes. *Open Biol.* **2021**, *10* (9), 200209. https://doi.org/10.1098/rsob.200209.

(9) Schoeman, D.; Fielding, B. C. Coronavirus Envelope Protein: Current Knowledge. *Virol. J.* **2019**, *16* (1), 69. https://doi.org/10.1186/s12985-019-1182-0.

(10) Cavanagh, D. Coronaviridae: A Review of Coronaviruses and Toroviruses BT -

Coronaviruses with Special Emphasis on First Insights Concerning SARS; Schmidt, A., Weber, O., Wolff, M. H., Eds.; Birkhäuser Basel: Basel, 2005; pp 1–54. https://doi.org/10.1007/3-7643-7339-3_1.

(11) McBride, R.; Van Zyl, M.; Fielding, C. B. The Coronavirus Nucleocapsid Is a Multifunctional Protein. *Viruses* . 2014. https://doi.org/10.3390/v6082991.

(12) Tiwari, V.; Beer, J. C.; Sankaranarayanan, N. V.; Swanson-Mungerson, M.; Desai, U. R. Discovering Small-Molecule Therapeutics against SARS-CoV-2. *Drug Discov. Today* **2020**, *25* (8), 1535–1544. https://doi.org/https://doi.org/10.1016/j.drudis.2020.06.017.

(13) Mohamed, K.; Yazdanpanah, N.; Saghazadeh, A.; Rezaei, N. Computational Drug Discovery and Repurposing for the Treatment of COVID-19: A Systematic Review. *Bioorg. Chem.* **2021**, *106*, 104490. https://doi.org/https://doi.org/10.1016/j.bioorg.2020.104490.

(14) Chilamakuri, R.; Agarwal, S. COVID-19: Characteristics and Therapeutics. *Cells* . 2021. https://doi.org/10.3390/cells10020206.

(15) Chen, P.; Nirula, A.; Heller, B.; Gottlieb, R. L.; Boscia, J.; Morris, J.; Huhn, G.; Cardona, J.; Mocherla, B.; Stosor, V.; Shawa, I.; Adams, A. C.; Van Naarden, J.; Custer, K. L.; Shen, L.; Durante, M.; Oakley, G.; Schade, A. E.; Sabo, J.; Patel, D. R.; Klekotka, P.; Skovronsky, D. M. SARS-CoV-2 Neutralizing Antibody LY-CoV555 in Outpatients with Covid-19. *N. Engl. J. Med.* **2020**, *384* (3), 229–237. https://doi.org/10.1056/NEJMoa2029849.

(16) Weinreich, D. M.; Sivapalasingam, S.; Norton, T.; Ali, S.; Gao, H.; Bhore, R.; Musser, B. J.; Soo, Y.; Rofail, D.; Im, J.; Perry, C.; Pan, C.; Hosain, R.; Mahmood, A.; Davis, J. D.; Turner, K. C.; Hooper, A. T.; Hamilton, J. D.; Baum, A.; Kyratsous, C. A.; Kim, Y.; Cook, A.; Kampman, W.; Kohli, A.; Sachdeva, Y.; Graber, X.; Kowal, B.; DiCioccio, T.; Stahl, N.; Lipsich, L.; Braunstein, N.; Herman, G.; Yancopoulos, G. D. REGN-COV2, a Neutralizing Antibody Cocktail, in Outpatients with Covid-19. *N. Engl. J. Med.* **2020**, *384* (3), 238–251. https://doi.org/10.1056/NEJMoa2035002.

(17) Singh Tomar, P. P.; Arkin, I. T. SARS-CoV-2 E Protein Is a Potential Ion Channel That Can Be Inhibited by Gliclazide and Memantine. *Biochem. Biophys. Res. Commun.* **2020**, *530* (1), 10–14. https://doi.org/https://doi.org/10.1016/j.bbrc.2020.05.206.

(18) Das, G.; Das, T.; Chowdhury, N.; Chatterjee, D.; Bagchi, A.; Ghosh, Z. Repurposed Drugs and Nutraceuticals Targeting Envelope Protein: A Possible Therapeutic Strategy against COVID-19. *Genomics* **2021**, *113* (1, Part 2), 1129–1140. https://doi.org/https://doi.org/10.1016/j.ygeno.2020.11.009.

(19) Monje-Galvan, V.; Voth, G. A. Molecular Interactions of the M and E Integral Membrane Proteins of SARS-CoV-2. *bioRxiv* **2021**, 2021.04.29.442018. https://doi.org/10.1101/2021.04.29.442018.

(20) Yu, A.; Pak, A. J.; He, P.; Monje-Galvan, V.; Casalino, L.; Gaieb, Z.; Dommer, A. C.; Amaro, R. E.; Voth, G. A. A Multiscale Coarse-Grained Model of the SARS-CoV-2 Virion. *Biophys. J.* **2021**, *120* (6), 1097–1104. https://doi.org/10.1016/j.bpj.2020.10.048.

(21) Heo, L.; Feig, M. Modeling of Severe Acute Respiratory Syndrome Coronavirus 2 (SARS-CoV-2) Proteins by Machine Learning and Physics-Based Refinement. *bioRxiv*

2020, 2020.03.25.008904. https://doi.org/10.1101/2020.03.25.008904.

(22) Michaud-Agrawal, N.; Denning, E. J.; Woolf, T. B.; Beckstein, O. MDAnalysis: A Toolkit for the Analysis of Molecular Dynamics Simulations. *J. Comput. Chem.* **2011**, *32* (10), 2319–2327. https://doi.org/https://doi.org/10.1002/jcc.21787.

(23) Gapsys, V.; de Groot, B. L.; Briones, R. Computational Analysis of Local Membrane Properties. *J. Comput. Aided. Mol. Des.* **2013**, *27* (10), 845–858. https://doi.org/10.1007/s10822-013-9684-0.

(24) Van Der Spoel, D.; Lindahl, E.; Hess, B.; Groenhof, G.; Mark, A. E.; Berendsen, H. J. C. GROMACS: Fast, Flexible, and Free. *J. Comput. Chem.* **2005**, *26* (16), 1701–1718. https://doi.org/https://doi.org/10.1002/jcc.20291.

(25) Huang, J.; MacKerell Jr, A. D. CHARMM36 All-Atom Additive Protein Force Field: Validation Based on Comparison to NMR Data. *J. Comput. Chem.* **2013**, *34* (25), 2135–2145. https://doi.org/https://doi.org/10.1002/jcc.23354.

(26) Price, D. J.; Brooks, C. L. A Modified TIP3P Water Potential for Simulation with Ewald Summation. *J. Chem. Phys.* **2004**, *121* (20), 10096–10103. https://doi.org/10.1063/1.1808117.

(27) Hess, B.; Bekker, H.; Berendsen, H. J. C.; Fraaije, J. G. E. M. LINCS: A Linear Constraint Solver for Molecular Simulations. *J. Comput. Chem.* **1997**, *18* (12), 1463–1472. https://doi.org/https://doi.org/10.1002/(SICI)1096-987X(199709)18:12<1463::AID-JCC4>3.0.CO;2-H.

(28) Essmann, U.; Perera, L.; Berkowitz, M. L.; Darden, T.; Lee, H.; Pedersen, L. G. A Smooth Particle Mesh Ewald Method. *J. Chem. Phys.* **1995**, *103* (19), 8577–8593. https://doi.org/10.1063/1.470117.

(29) Birdsall, C. K.; Langdon, A. B. *Plasma Physics via Computer Simulation*; Series in Plasma Physics and Fluid Dynamics; Taylor & Francis, 2004.

(30) Fliege, J.; Svaiter, B. F. Steepest Descent Methods for Multicriteria Optimization. *Math. Methods Oper. Res.* **2000**, *51* (3), 479–494. https://doi.org/10.1007/s001860000043.

(31) Evans, D. J.; Holian, B. L. The Nose–Hoover Thermostat. *J. Chem. Phys.* **1985**, *83* (8), 4069–4074. https://doi.org/10.1063/1.449071.

(32) Parrinello, M.; Rahman, A. Polymorphic Transitions in Single Crystals: A New Molecular Dynamics Method. *J. Appl. Phys.* **1981**, *52* (12), 7182–7190. https://doi.org/10.1063/1.328693.